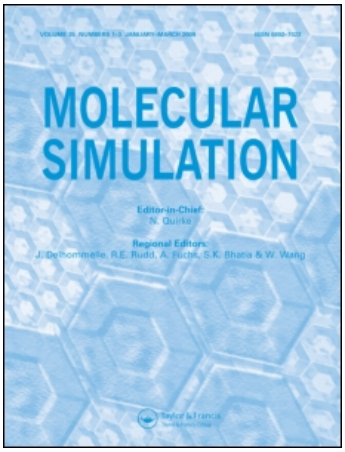

Molecular Simulation
Publication details, including instructions for authors and subscription information:
http://www.informaworld.com/smpp/title~content=t713644482

Molecular dynamics simulations of three protegrin-type antimicrobial peptides: interplay between charges at the termini, β-sheet structure and amphiphilic interactions

D. S. Bolintineanu[a]; A. A. Langham[a]; H. T. Davis[a]; Y. N. Kaznessis[a]
[a] Department of Chemical Engineering and Materials Science, University of Minnesota, Minneapolis, MN, USA

To cite this Article Bolintineanu, D. S. , Langham, A. A. , Davis, H. T. and Kaznessis, Y. N.(2007) 'Molecular dynamics simulations of three protegrin-type antimicrobial peptides: interplay between charges at the termini, β-sheet structure and amphiphilic interactions', Molecular Simulation, 33: 9, 809 — 819
To link to this Article: DOI: 10.1080/08927020701393481
URL: http://dx.doi.org/10.1080/08927020701393481

Molecular Simulation, Vol. 33, Nos. 9–10, 15–30 August 2007, 809–819

Taylor & Francis
Taylor & Francis Group

Molecular dynamics simulations of three protegrin-type antimicrobial peptides: interplay between charges at the termini, β-sheet structure and amphiphilic interactions

D. S. BOLINTINEANU†, A. A. LANGHAM†, H. T. DAVIS† and Y. N. KAZNESSIS†‡*

†Department of Chemical Engineering and Materials Science, University of Minnesota, 421 Washington Ave SE, Minneapolis, MN 55455, USA
‡Digital Technology Center, University of Minnesota, 117 Pleasant St SE, Minneapolis, MN 55455, USA

(Received January 2007; in final form March 2007)

We have carried out molecular dynamics simulations of the naturally occurring protegrin PG-1 peptide and two of its mutants, PC-9 and PC-13 in the presence of a dodecyl-phosphocholine (DPC) micelle. The effects of mutations that disrupt the β-sheet structure in the case of PC-9 and reduce the charge at the C-terminus in the case of PC-13 are analyzed. It is found that the surface-bound conformations of the peptides are severely affected by both mutations. PG-1 exhibits a conformation in which the C-terminus and the β-hairpin turn interact strongly with the micelle lipid head groups, while its N-terminal strand bends away from the micelle and resides in the aqueous region; PC-13 exhibits strong interactions with the micelle at its N-terminus as well as the β-hairpin turn region, while retaining a much more compact conformation than PG-1; PC-9 achieves a highly distorted conformation relative to the homologous PG-1 structure, which allows both its termini and the β-hairpin region to interact with the micelle. These significant differences observed as a result of seemingly minor mutations to the sequences of the three peptides are explained in terms of the interplay between residue charges, structural rigidity and amphiphilic interactions. Conservative inferences are made bridging these biophysical interactions and the pharmacological profiles of the peptides.

Keywords: Molecular dynamics simulations; Protegrin; DPC micelle; Antimicrobial peptides; β-Hairpin

1. Introduction

Antimicrobial peptides (AMPs) are a diverse class of nautrally occurring, relatively small proteins that exhibit a broad range of antimicrobial, antifungal and antiviral activities [1]. Since the discovery of magainin in the skin of the African clawed frog *Xenopus laevis* twenty years ago [2], hundreds of AMPs have been isolated from all types of living organisms, ranging from microbes and plants to fish, birds and mammals (including humans) [3,4]. As a result of the growing resistance of many common bacterial strains to conventional antibiotics [5], there has been tremendous interest in the development of novel antibiotic agents based on AMPs [1,3,4,6]. AMPs are particularly promising because they interact primarily with the cellular membrane of their target microbe rather than a specific cytosolic target [1,3,4,6]; as such, it is far less likely that bacteria will develop significant resistance to AMPs. This hypothesis has been substantiated by several studies that unsuccessfully attempted to confer AMP resistance to bacterial strains by *in vitro* treatment with sub-inhibitory concentrations [7]. However, many potent AMPs also exhibit considerable toxicity to host cells at the concentration levels required for the effective treatment of microbial infections [3,8]. Currently, this represents a significant bottleneck in the development of AMPs into clinical antibiotics. The exact mechanism of action of AMPs has not been sufficiently clarified to empower the rational design of peptides that exhibit low toxicity to host cells, while retaining their high activity against bacterial cells.

Several mechanisms have been proposed for the action of AMPs, which will not be discussed in detail here (for thorough reviews, the reader is referred to references [3,6,9]). All of these models agree that the initial step in the cytolytic process is the binding of the peptide to the lipid membrane surface. As such, positively charged residues such as arginine or lysine are presumed to be

*Corresponding author. Tel.: + 1-612-624-4945. Fax: + 1-612-626-7246. Email: yiannis@cems.umn.edu

Molecular Simulation
ISSN 0892-7022 print/ISSN 1029-0435 online © 2007 Taylor & Francis
http://www.tandf.co.uk/journals
DOI: 10.1080/08927020701393481

responsible for the selectivity of AMPs toward the anionic surfaces of bacterial membranes over zwitterionic mammalian cell membranes [6,9,10]. However, mutations that increase the net charge do not necessarily result in proportionally higher activity, nor do they allow moderation of toxicity [11]. This suggests a more complex mechanism that necessitates an atomic-level investigation. Molecular dynamics simulations provide an excellent tool for such studies, and have been used extensively in the past to study various peptide–membrane systems [12]. In the present work, we have carried out such a study for three protegrin-type AMPs.

Protegrins are a promising class of AMPs characterized by a β-hairpin structure, originally isolated from porcine neutrophils [13]. Protegrins are highly active against a variety of Gram-positive and Gram-negative bacteria, but also exhibit significant toxicity towards human red blood cells and epithelial cells. The most common naturally occurring protegrin, designated as PG-1 (RGGRL CYCRR RFCVC VGR-NH_2), has been the subject of numerous experimental investigations aimed at probing its mechanism of interaction with cell membranes. Its solution structure [14] as well as its dimerized structure in a 1-palmitoyl-2-oleoyl-phosphatidylcholine (POPC) bilayer [15] and a dodecyl-phosphocholine (DPC) micelle [16] have been resolved by NMR experiments; its orientation and insertion in dilauroyl-phosphatidylcholine (DLPC) and interactions with other lipid bilayers have been reported in great detail [17,18]; numerous mutated analogues of protegrin-1 have been synthesized, and their activity and toxicity have been reported [19]. Such experimental investigations are invaluable both as input and validation for molecular dynamics simulations of these systems.

Previous work in our group has focused on simulations aimed at elucidating the structural characteristics and molecular interactions responsible for the antimicrobial activity and host-cell toxicity of a variety of AMPs. In particular, we have had significant success with simulations of detergent micelles as membrane mimicking environments. While such simulations with a single peptide cannot access the latter steps of the proposed cell lysing process (peptide oligomerization, pore formation and membrane destabilization), they can be useful in capturing the relevant features of the initial peptide–membrane binding process. Recent experimental work by Mani *et al.* [20] suggests that PG-1 binds to mammalian membranes in a carpet-like fashion, and its cytotoxic action is thus likely the result of a carpet-like mechanism. Although their model membrane consisted of a bilayer composed of a 1.2:1 mixture of POPC and cholesterol, which differs in both chemistry and geometry from DPC micelles, we hypothesize that the essential features of a zwitterionic surface rich in phosphocholine moieties can be at least partially captured by a DPC micelle. Even if the mechanism of action against mammalian cells is not carpet-like, the initial membrane binding process is still an important phenomenon.

Furthermore, simulations with micelles circumvent the computational expense and methodological issues associated with lipid bilayers, while retaining the relevant biophysical characteristics of an amphiphilic environment: a hydrophobic, aliphatic core surrounded by a flexible, hydrophilic interface. For instance, there has been significant debate in literature as to the correct statistical mechanical ensemble for use in bilayer simulations, particularly with regards to the appropriate applied surface tension [21–23]. For the CHARMM force field employed in the current work [24], the NP_zAT or $NP_Z\gamma T$ ensembles are recommended for bilayer systems [25,26]. In the former, the area of the bilayer patch is kept constant, while the simulation box is allowed flexibility in the direction normal to the bilayer plane in order to adjust the *z*-component of the pressure to the required value; in the latter, a surface tension constrain is applied to the bilayer while allowing fluctuations in box size in all directions. Simulations of a membrane-bound peptide in the NP_ZAT ensemble limit the peptide to conformations and orientations that correspond to a constant projected area; thus, some knowledge of the membrane-bound conformation and orientation of the peptide is required a priori. Conversely, it is not clear what the correct value of the applied surface tension should be for simulations in the $NP_z\gamma T$ ensemble [25,27], particularly for a small bilayer patch with an embedded peptide. Lipid bilayer simulations are further encumbered by the much slower relaxation time of lipid molecules in bilayers as compared to micelles [28–32], which would require much longer simulation times to sample relevant peptide conformations. For further discussion of the benefits and shortcomings of micelles as membrane mimics, the reader is referred to references [12,33].

As already mentioned, DPC micelles represent a significant simplification of real cell membranes, which consist of lipid bilayers composed of complex mixtures of phospholipids, cholesterol, membrane-bound proteins and numerous other compounds. Although the differences in chemistry, energetics and geometry between DPC micelles and real cell membranes are vast, we aim to investigate whether these simple models are able to capture some of the relevant features of peptide–membrane interactions. The present work is part of a continued effort in such investigations, and aims to compare the structural features and relevant interactions of two protegrin analogues and the naturally occurring PG-1.

The two synthetic analogues selected for the present study are PC-9 (RGGRL AYCRR RFCVA VGR-NH_2) and PC-13 (RGGRL CYCRR RFCVC V-NH_2). The difference between PC-9 and the naturally occurring PG-1 consists of the replacement of Cys^6 and Cys^{15} by alanine residues. This removes one of the two cysteine–cysteine disulfide bonds from the hairpin, a critical structural feature that helps stabilize the β-hairpin structure of PG-1. The mutation involved in the synthesis of PC13 leads to the absence of the Gly^{17} and Arg^{18} residues found at the C-terminus of PG-1. This results in a shortening

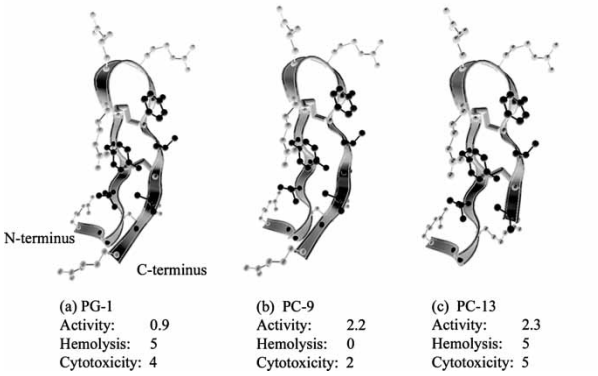

Figure 1. Starting structures of the three peptides. The backbone is shown as a grey ribbon, and disulfide bonds as thick grey bonds. Arginine side chains are shown in grey CPK (ball-and-stick) representation; other side chains are shown in black CPK. See text for explanation of activity, hemolysis and cytotoxicity values.

of the C-terminal strand of the hairpin, and a decrease in the net charge of the peptide (due to the absence of Arg_{18}). The available antibacterial activity and toxicity measurements for all three peptides are summarized along with their initial structures in figure 1.

The activity measurements indicate the minimum peptide concentration required to inhibit the growth of *Escherichia coli*, while cytotoxicity and hemolysis values correspond to a scale from 0 to 5, with 0 being least cytotoxic/hemolytic, and 5 being most cytotoxic/hemolytic. Thus, a lower value in the activity entries of figure 1 indicates high levels of antimicrobial activity, while a higher cytotoxicity/hemolysis value indicates higher toxicity. A desirable drug candidate would have low values in all columns. As shown, the two mutants have very similar activity against *E. coli*, and both are somewhat less active than PG-1, but not significantly so. However, while PG-1 and PC-13 are highly toxic, PC-9 displays markedly reduced toxicity against both red blood cells and epithelial cells. While our simplified model cannot be expected to fully explain these data, the overall toxicity ranking will be kept in mind for the analysis of our simulations.

2. Methodology

All simulations and analysis were carried out using the CHARMM software package version c29b2 [34] with the param22 all-atom force field [24]. The topology and parameters for DPC were obtained by combining the dodecyl chain of dodecylsulfate with the phosphocholine head group. The starting coordinates for the micelle were obtained from molecular dynamics simulations carried out by Kamath and Wong [30]. Previous simulations of peptide–micelle systems carried out by our group [12,33,35–37] indicate that a single DPC molecule frequently separates from the main micelle relatively quickly in the presence of a peptide. As such, a single molecule was removed, resulting in a micelle composed of 59 molecules. The starting structure of PG-1 was obtained from its NMR solution structure [14] in the RCSB Protein Databank [38] (pdb entry 1PG1). The starting structures of PC-9 and PC-13 were obtained through homology modeling based on the structure of PG-1 [19].

The simulation setup and production runs were similar for all three peptides, and will not be discussed separately. In all three cases, the peptide was initially placed so that its centre of mass coincided with the centre of mass of the micelle. As a result of the micelle's spherical symmetry, this placement avoids any orientational bias in the initial configuration of the system. The peptide–micelle complex was solvated in a rhombic dodecahedron simulation box of dimension 68.5 Å (this dimension represents the distance between the centres of adjacent box images). The complete solvated system in each simulation consisted of 6120 water molecules modeled using the TIP3 potential [39], 59 DPC molecules, the peptide, appropriate chloride counterions to neutralize the total system charge, and additional sodium and chloride ions, for a total of ~22,000 atoms.

The full system was minimized in a series of steepest descent minimizations, in which the peptide and water molecules were subjected to positional harmonic restraints of gradually decreasing strength, as described in previous work [12,33,35,36,40]. The system was then gradually heated to 303.15 K in 20,000 dynamics steps. All dynamics runs were carried out in the NPT (constant number of atoms, constant pressure and constant temperature) ensemble, using the extended system method based on the work of Andersen [41], Nosé [42,43] and Hoover [44] as implemented in the CHARMM NPT module. The pressure was set to 1.0 atm, with the piston mass array components all set to 250 amu for the heating phase, and 500 amu for the main production phase. The temperature was set to 303.15 K, with a thermal piston mass of 1800 kcal mol^{-1} ps^2. SHAKE constraints [45] were implemented for all bonds involving hydrogen atoms, including a fictitious bond between the hydrogen atoms of water in order to constrain the H—O—H angle. This allows for an integration time step of 2 fs. Particle mesh Ewald summation [46] was used for the treatment of electrostatic forces, with a real-space cut off of 11 Å, a real-space Gaussian width of 0.25 $Å^{-1}$, 4th order β-spline interpolation, and a FFT grid of about one point per Å. Van der Waals potential energy terms were shifted so as to equal zero at 11 Å. Non-bond and image lists were cut off at 13 Å, and updated every 25 steps. Periodic boundary conditions were applied in all directions. Coordinate snapshots were saved every 2 ps, which is the same sampling frequency used for data analysis unless otherwise noted. Simulations were run until the most relevant surface-bound configurations of the peptides were adequately sampled. This is explained in further detail below.

3. Results and discussion

For all three peptides, the sampling of most structural properties was performed starting from the point at which

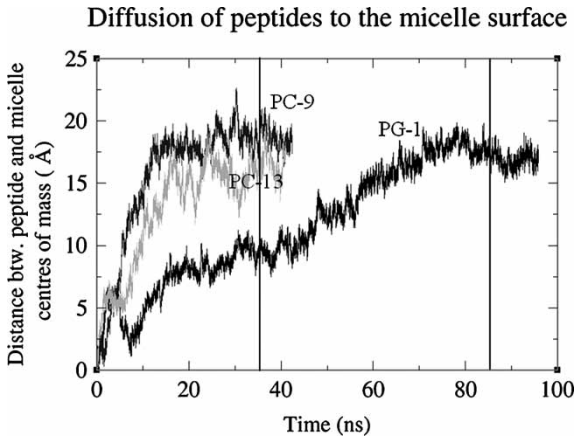

Figure 2. Plots of the distance between the peptide and micelle centres of mass for all three peptides. The vertical lines indicate the times beyond which equilibrium properties were sampled (35 ns for PC-9 and PC-13, 85 ns for PG-1).

the peptide reached a stable location with respect to the micelle. Since one of the slower relevant motions is the translational diffusion of the peptide from the interior to the surface of the micelle, this was taken as one of the primary indicators of a stabilized system. Figure 2 below shows the distance between the centre of mass of the micelle and the centre of mass of the peptide for all three systems studied. In previous work in our group with ovispirin [36,47] and protegrin [35], we have conducted simulations with different initial system configurations, starting the peptide in the micelle interior as well as in the aqueous phase. In all cases, convergence to the same position relative to the micelle was achieved relatively quickly. As such, we have a high degree of confidence that the present simulations represent well-converged results.

The systems are considered to have reached a stable conformation when there is no significant net change in the separation between peptide and micelle, corresponding to the flatter portion of the curves in figure 2. As seen, this took approximately 30 ns for PC-9 and PC-13, and 80 ns for PG-1. The significantly slower dynamics of PG-1 as compared to the two synthetic mutants may be indicative of a higher affinity for the hydrophobic micelle core; however, since the initial placement of the peptide at the centre of the micelle is not physically realistic, one cannot draw significant conclusions from the initial dynamics alone. As such, the comparison between the three systems will be carried out primarily based on properties measured starting from the time at which the stable configurations are reached. This time was taken to be 35 ns for PC-9 and PC-13 and 85 ns for PG-1.

3.1 Final peptide positions and orientations

The relative binding strength between peptide mutants and a DPC micelle is of particular interest, since the mechanism of action relevant to toxicity involves the peptide binding to a zwitterionic lipid/water interface. All three peptides were observed to migrate to the micelle surface, where they remained partially embedded into the micelle, and partially exposed to water, as expected for these amphiphilic systems. The distances of separation between the peptide and micelle centres of mass after equilibration are summarized for all three systems in table 1 below.

These data appear to correlate well with available toxicity data, wherein the least toxic PC-9 mutant resides farthest from the micelle centre, while the other two peptides have similar toxicities and reside at similar distances from the micelle. While no conclusive correlation between this separation distance and toxicity data can be made from so small a data set, this feature perhaps holds interest for future work. Figure 3 shows typical snapshots of the peptide–micelle systems following initial equilibration.

PG-1 adopts an orientation in which its β-sheet plane lies roughly tangent to the micelle surface, with a preference for the insertion of the C-terminal strand. Its two termini are spread significantly apart from one another. The C-terminal strand and the β-hairpin turn region interact with the micelle surface, while the N-terminus is bent away from the main structure, and resides primarily in the aqueous phase. PC-9, which lacks the stabilizing disulfide bond farthest from the hairpin turn, exhibits a curled conformation that is highly distorted from its initial structure. As seen in figure 3(b)), both termini, as well as the turn region interact with the micelle surface; however, this places a significant portion of the peptide chain in a loop that largely resides outside of the micelle. Finally, PC-13 adopts a conformation in which the majority of its C-terminal strand is embedded within the micelle, while residues near its N-terminus are also able to bend and interact with the micelle surface.

3.2 Peptide structure

As expected, the removal of the Cys^6–Cys^{15} disulfide bond in PC-9 has a significant effect on the peptide's structural characteristics. Plots of the root mean square deviation (RMSD) relative to the starting structure are shown for all three peptides in figure 4, as measured from the start of the simulations. Clearly, the deviation is more significant for PC-9, which may indicate a more significant effect of surface binding on the structure of PC-9, or simply that homology modeling for the initial structure is less successful for this peptide. In either case, significant overall structural changes are observed

Table 1. Mean distances of separation between the peptide and micelle centres of mass for all three systems.

Peptide	*Mean distance from micelle centre (in Å; fluctuations in braces)*
PG-1	16.57 (1.16)
PC-9	18.63 (0.86)
PC-13	16.91 (0.25)

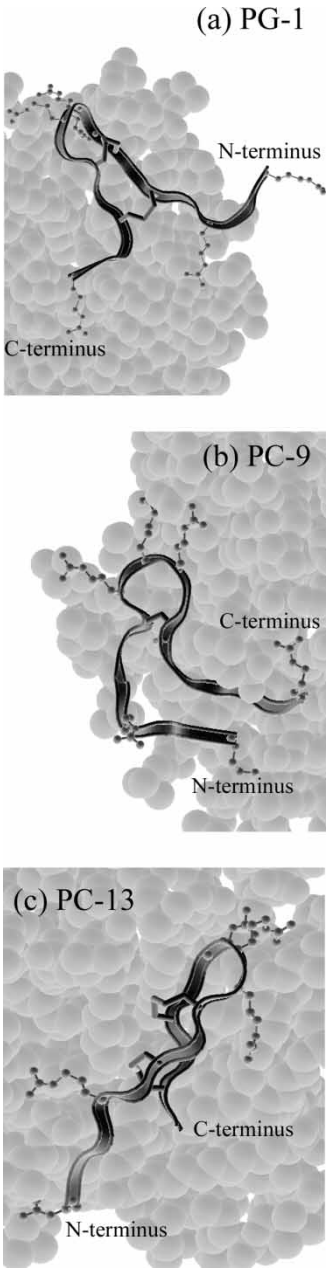

Figure 3. Equilibrated surface-bound conformations of all three peptides. Backbone structures are shown as dark ribbons; cysteine–cysteine disulfide bonds are shown as thick, dark bonds; arginine side chains are shown in grey CPK (ball-and-stick) representations; the micelle is partially shown in light grey VDW (spheres) representations. Side chains other than arginine have been excluded for clarity.

as compared to the other two peptides. The primary difference can be visually observed as a significant overall bending of the β-hairpin, as well as a curl in the N-terminal strand (around residues 5–7), as depicted in figure 3. Interestingly, the fluctuations in the RMSD values in the stable membrane-bound state are smaller for PC-9 than for the other peptides (0.16 Å for PC-9 as opposed to 0.20 Å for PC-13 and 0.49 Å for PG-1, as measured only beyond the equilibration times indicated above). These results indicate that while PC-9 deviates from the starting β-hairpin structure more significantly, it is eventually able

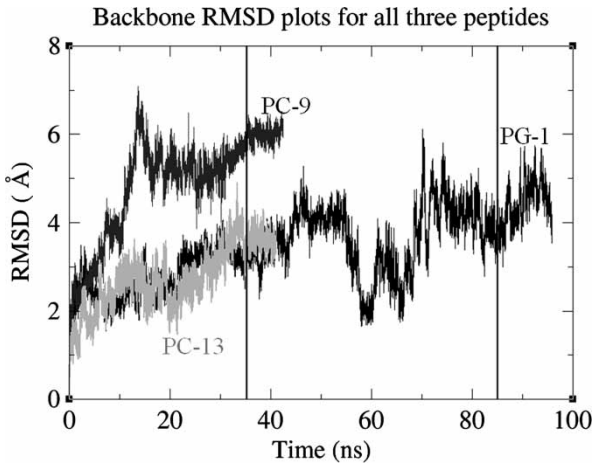

Figure 4. Backbone RMSD of all three peptides relative to their starting structures. The vertical lines indicate the times beyond which equilibrium properties were sampled (35 ns for PC-9 and PC-13, 85 ns for PG-1), including the reported RMSD fluctuations (see text).

to adopt a more stable surface-bound conformation than the other two peptides. As such, it would seem that the absence of the stabilizing effect of the Cys^6–Cys^{15} disulfide bond in PC-9 allows this peptide other interactions that ultimately lead to a more stable backbone conformation than the native PG-1 or PC-13. These interactions are presented in detail in the "Peptide–micelle interactions" section below.

More detailed insight into the structural characteristics of the three peptides can be gained from an analysis of the backbone dihedral angles. The two dihedral angles most relevant to peptide backbone conformations are φ and ψ, defined in the usual way: φ is the dihedral angle formed by backbone atoms C'_{i-1}—N_i—C^{α}_i—C'_i (i.e. torsion around the N_i—C^{α}_i bond), and ψ is the dihedral angle formed by atoms N_i—C^{α}_i—C'_i—N_{i+1} (i.e. torsion around the C^{α}_i—C'_i bond). The index i represents the position in the amino acid sequence, which also corresponds to the index of φ and ψ values as presented in figure 6. Figure 5 depicts the definition of the dihedral angle φ.

The mean values and fluctuations of the dihedral angles are shown in figure 6 for all three peptides, as measured only for the stabilized surface-bound conformations. Values of φ between $-90°$ and $-140°$ and ψ between 120° and 180°, or below $-160°$ are typical of a β-sheet structure.

As expected, these values are prevalent in both PG-1 and PC-13, with the exception of residues 9–11, which correspond to the turn of the β-hairpin, and the residues near the termini. Notably, PC-9, which lacks the Cys^6–Cys^{15} disulfide link that stabilizes the β-sheet structure in both PG-1 and PC-13, shows several dihedral angles outside of the typical β-sheet range, in addition to the region of the β-hairpin turn and the termini. Positions 7 and 13 of PC-9 have ψ values around $-117°$ and $-54°$, respectively, both outside of the typical β-sheet range. Additionally, φ_7 has a value of around 103°, also atypical of β-sheet structure. Comparison to PG-1 and PC-13 show that these residues are β-sheet in the case of peptides with

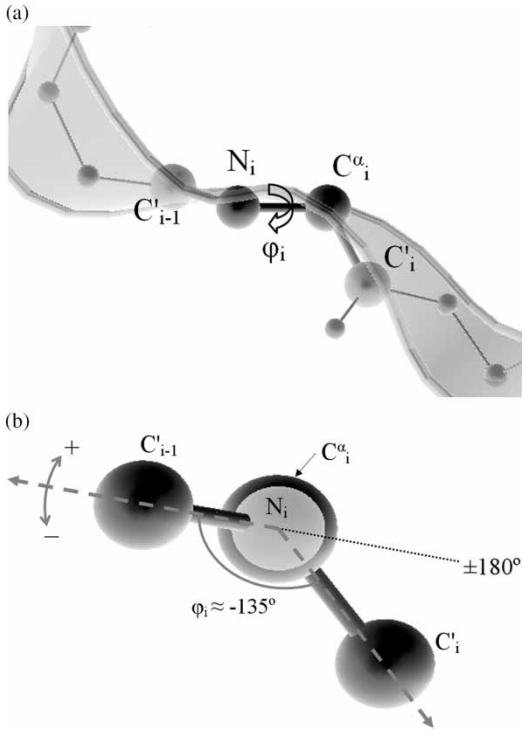

Figure 5. (a) Close-up side-view of a section of the peptide backbone depicting the definition of the dihedral angle φ_i. The four relevant atoms are shown as larger spheres, while the ribbon representation corresponds to overall backbone structure. The dihedral angle φ is defined as the torsion angle around the N_i—C_i^α bond; equivalently, this is the angle between the normal of the plane containing atoms C'_{i-1}, N_i, C_i^α and the normal of the plane containing C'_i, C_i^α, N_i. The dihedral angle ψ_i is similarly defined, but for the sequence N_i—C_i^α—C'_i—N_{i+1}. (b) View along the N_i—C_i^α bond, from N_i towards C_i^α. Following convention, the dihedral angle φ_i is defined as positive in a clockwise direction about the N_i—C_i^α vector, and ranges from $-180°$ to 180°. The dihedral angle ψ_i is similarly defined, but for the sequence N_i—C_i^α—C'_i—N_{i+1}.

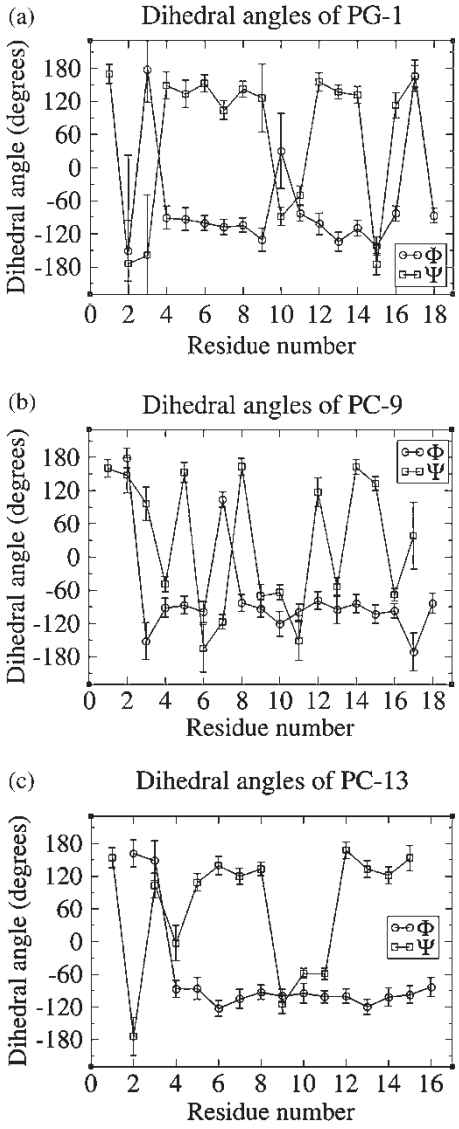

Figure 6. (a) Dihedral angle data of PG-1. The predominant β-sheet structure is seen throughout the length of the peptide backbone, with the exception of residues 9–11 (the β-hairpin turn region), as well as the two termini. Note the large fluctuations in the dihedral angles near the N-terminus. (b) Dihedral angle data of PC-9. The well-defined β-sheet structure seen in PG-1 and PC-13 is much less apparent here. Fluctuations are significantly smaller than for PG-1. (c) Dihedral angle data of PC-13. Note the well-defined β-sheet structure, also seen in PG-1. Fluctuations are much smaller than in PG-1.

two disulfide bonds. These differences correspond to the bending of the two strands of the hairpin in PC-9 discussed above, as well as a curling of the N-terminal strand between residues 5 and 7, neither of which can happen in the more rigid structures of PG-1 and PC-13. Another notable feature of the dihedral angle plots are the higher deviations in the values of the dihedral angles observed for PG-1, in particular near the N-terminus (residues 1–3). This corresponds to the high flexibility of the backbone of this region of PG-1, which remains well outside of the micelle core, and interacts freely with the less viscous bulk solvent. In contrast, PC-9 and PC-13 exhibit significantly smaller dihedral angle fluctuations, indicating the more stable structures of these two peptides, an effect that was also noted in the fluctuations of RMSD values.

3.3 Peptide–micelle interactions

The following discussions refer exclusively to properties measured beyond the times at which the physically relevant surface-bound conformation is reached, as discussed previously. Sampling of all data was performed every 2 ps, with the exception of the radial distribution functions (RDFs) of water with respect to the individual peptide residues, which were sampled every 20 ps. RDFs of groups other than water have been normalized by an arbitrary bulk density of 0.01 atoms/Å^3; water distribution functions have been normalized by a bulk density of 0.034 molecules/Å^3 (corresponding to a density of 1 g/mL), and as such are the only RDFs that approach unity far from the reference site. In computing RDFs from the peptide side chains to various groups (figure 8(a)–(c)), no corrections were applied for the volume occupied by other peptide moieties near the reference site atoms (these are often referred to as excluded volume effects [48]). In cases where the reference site consists of multiple atoms (RDFs for individual residues of the peptide, figure 8(a)–(c)), the RDFs were normalized by the number of atoms in the

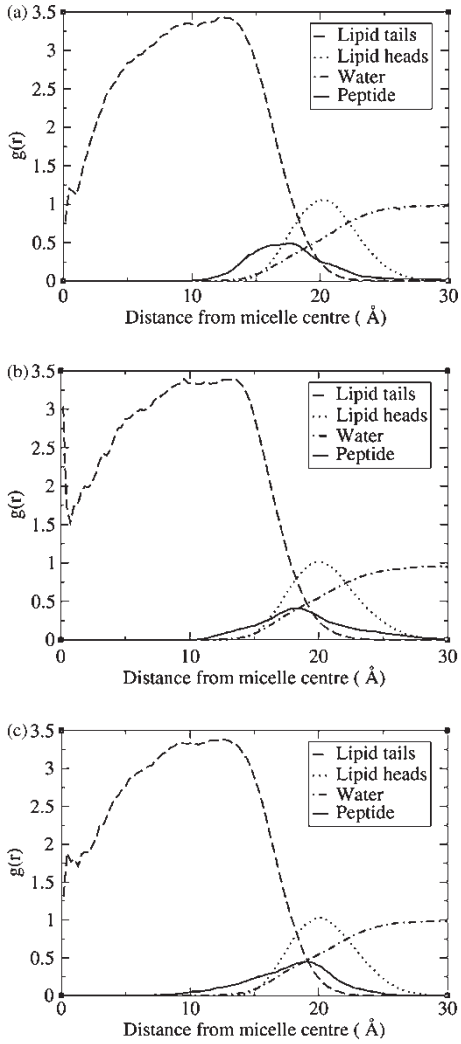

Figure 7. (a) RDFs of various groups from the centre of the micelle for PG-1. (b) RDFs of various groups from the centre of the micelle for PC-9. (c) RDFs of various groups from the centre of the micelle for PC-13.

reference site. The use of an arbitrary bulk density for various atomic groups, as well as the omission of excluded volume effects are justified in the present context, where RDFs are used only to compare the interactions of various moieties across the three systems of interest.

3.3.1 Overall structural characteristics. In order to compare the relevant interactions in the three systems, RDFs were first constructed for various groups from the centre of the micelle, shown in figure 7(a)–(c). These data serve to illustrate the overall structure of the solvated peptide–micelle complex. The head group atoms considered in the analysis were all of the atoms in the phosphate and choline groups, excluding hydrogen. The peptide group consists of all peptide atoms excluding hydrogen, and the tail group consists of the twelve carbon atoms of the aliphatic DPC tail.

As expected, the hydrophilic head group atoms are predominantly located at the surface of the micelle,

Table 2. Contacts between lipid head and tail groups and the three peptides for various ranges. All data have been normalized by the number of heavy atoms of each peptide.

	Lipid head contacts per heavy atom of peptide			*Lipid tail contacts per heavy atom of peptide*		
Peptide / *Distance*	*6 Å*	*8 Å*	*10 Å*	*6 Å*	*8 Å*	*10 Å*
PG-1	0.631	0.970	1.29	0.731	1.10	1.65
PC-9	0.622	0.920	1.19	0.709	1.05	1.50
PC-13	0.658	0.958	1.28	0.833	1.24	1.87

approximately 20 Å from the centre. The peptides are also generally located at the surface, where they are in close proximity to water, lipid head groups, as well as the aliphatic tails, displaying the expected amphiphilic behaviour. Water penetration into the micelle core does not extend beyond a distance of 10 Å from the micelle centre.

The distributions of the micelle head and tail atoms from the centre are similar in all three cases, as is the distribution of water molecules relative to the micelle, suggesting no significant differences in the overall structure of the micelle between the three simulations. The only notable differences are in the peptide distributions. PG-1 appears to have the strongest affinity for the micelle core, as seen by the large overlap of the distribution of most of its atoms with the lipid tail distribution. PC-13 exhibits a more spread out distribution with a lower peak, but extends further into the micelle core, reaching as close as 7.5 Å from the micelle centre. PC-9 has a peak intensity similar to PC-13, but does not have the same penetration depth, with the left tail of its distribution penetrating only as far as 10 Å from the micelle centre.

Overall, peptide–micelle interactions are also presented numerically in table 2. Contact numbers are defined as the number of atoms of the moiety of interest (e.g. lipid heads/tails) found within a specified distance from the reference site. Lipid head and tail atoms were defined as above, and contact numbers were calculated for ranges of 6, 8 and 10 Å from any of the heavy atoms of the peptides (i.e. any atoms except hydrogen). The contact numbers were then normalized by the number of heavy atoms in each peptide.

3.3.2 Specific peptide–micelle interactions. In order to investigate peptide–micelle interactions in further detail, RDFs were constructed from the individual residues of all peptides to the micelle head and tail groups, as well as water. The results are presented in figure 8(a)–(c). The reference sites were taken as the heavy atoms of the side chains of the residue in question, with the exception of glycine, for which the α-Carbon was used as the reference site. Head and tail moieties in the micelle were defined as before. Note that water RDFs do not approach unity here because the distance range does not extend past the micelle.

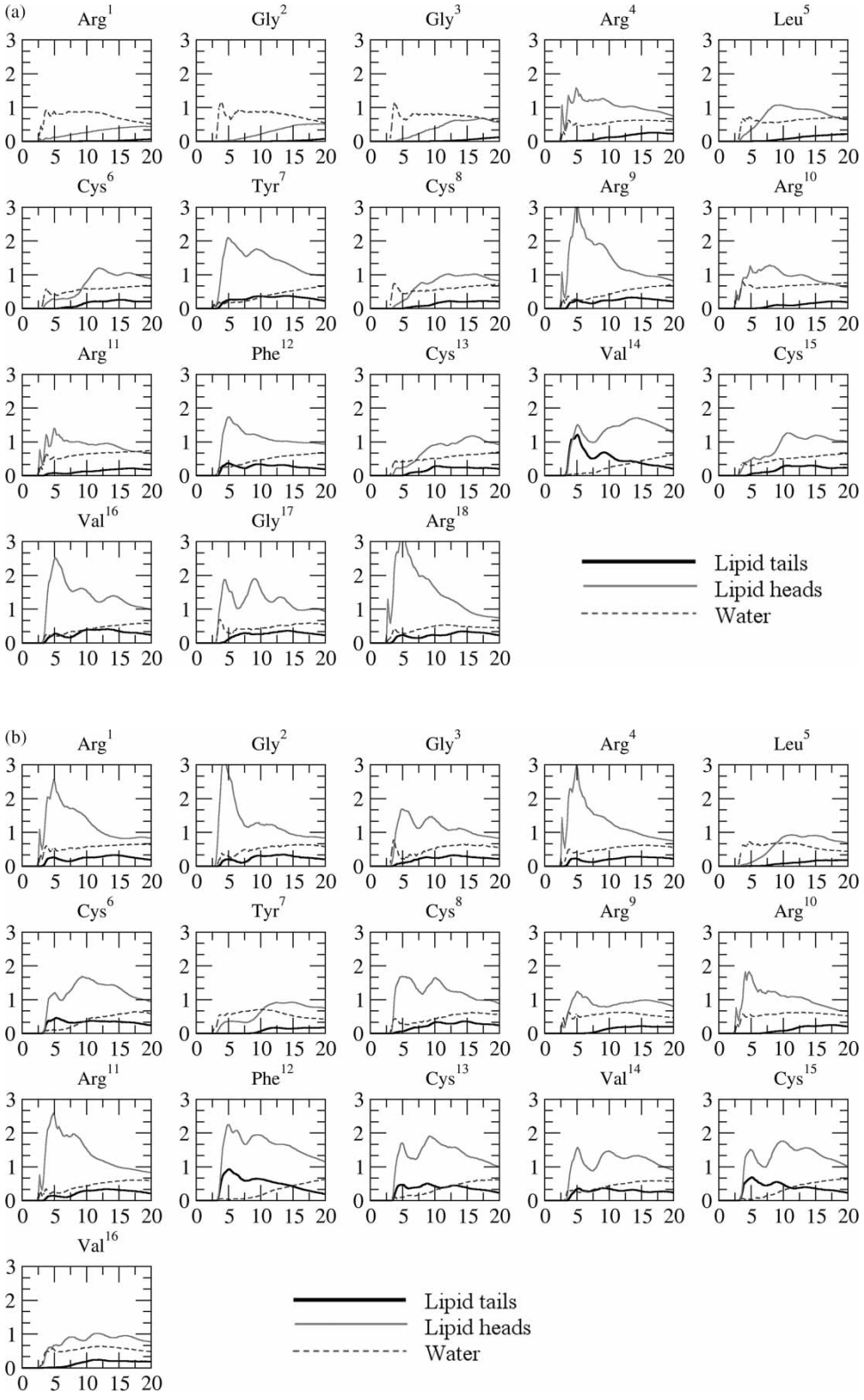

3.3.2.1 PG-1

The most striking feature of the RDFs of PG-1 residues are the low interactions between residues 1 and 3 and the micelle. This is initially surprising, since the positively charged Arg-1 residue, along with the protonated N-terminus, are expected to pull this relatively flexible portion of the peptide towards the zwitterionic interface. In particular, interactions between the guanidinium groups of arginine and the phosphate group of DPC can be expected.

However, as evidenced by the lower lipid peaks and larger water peaks in the RDFs of these residues, they primarily reside in the bulk water region. This is also clearly observed visually, as evidenced in figure 3 by the

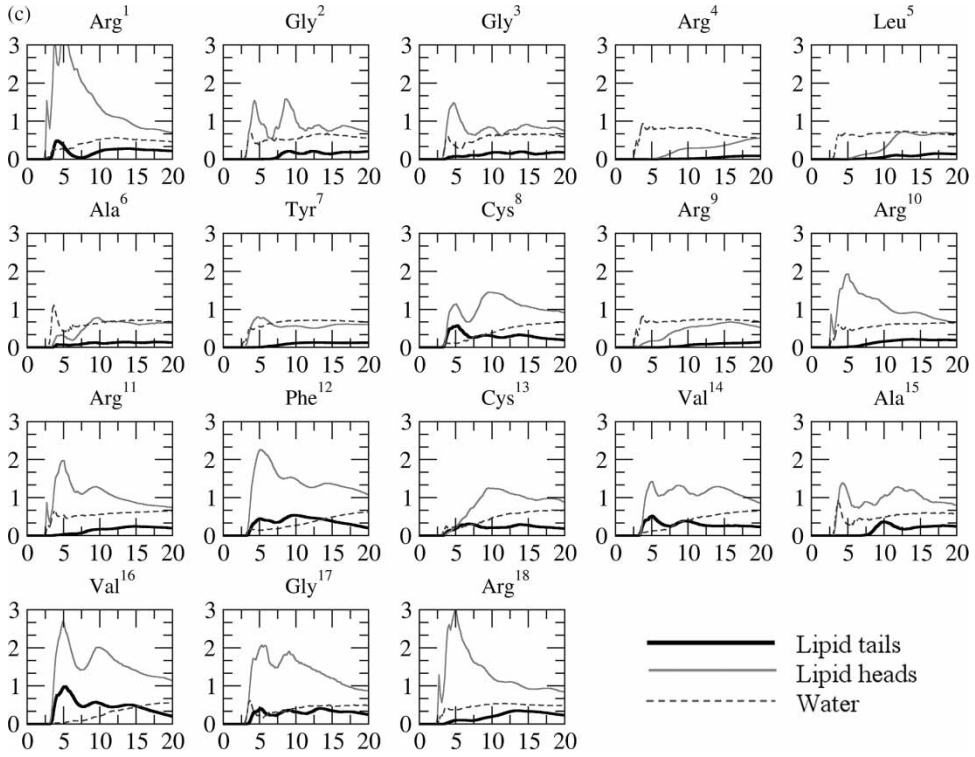

Figure 8. (a) RDFs of various groups from all residues of PG-1. The N-terminus (residues 1–3) has very limited interactions with the micelle, and resides primarily in the aqueous region. The arginine residues near the β-hairpin turn (residues 9–11) interact with the micelle head groups, as expected. (b) RDFs of various groups from all residues of PC-13. Both termini, as well as the β-hairpin turn are able to interact strongly with the micelle. (c) RDFs of various groups from all residues of PC-9. The N-terminus interacts strongly with the micelle, in stark contrast to PG-1.

significant bend in the N-terminus strand of the backbone away from the micelle. The strongest interactions with the micelle occur at the opposite terminus, between residues 16 and 18 and both the head and tail regions of the micelle, as evidenced by the high peaks in the RDFs. The highly charged β-turn region of the peptide also has a strong affinity towards the micelle surface, in particular Arg^{9} which exhibits a high peak. The strong attraction of the C-terminus and the hairpin turn region to the micelle surface appear to orient the peptide in such a way that residues 1–3 at its N-terminal strand are not able to favorably interact with the micelle. Furthermore, electrostatic repulsions between the two cationic termini may be responsible for the spreading observed.

3.3.2.2 PC-13

In stark contrast to PG-1, residues 1–3 of PC-13 exhibit very strong interactions with the micelle surface, while the C-terminus (namely Val^{16}) does not. This can be partially explained by considering that the mutation in PC-13 results in the absence of Gly^{17} and Arg^{18} from the C-terminus as compared to PG-1—as such, this terminus no longer possesses a positive charge, and will not interact with the micelle interface as strongly. Unlike in the case of PG-1, PC-13 is not forced into an orientation that places the opposing N-terminal strand into the water region. As a result, the N-terminal strand (residues 1–3) of PC-13 is more readily able to interact with the micelle surface, which explains the significant differences between the interactions of these residues in the two seemingly similar structures of PC-13 and PG-1.

It should also be noted that for cationic arginine residues to interact with the micelle, they must penetrate to a sufficient depth to interact with the anionic phosphate moieties, and not the cationic choline groups. If the overall orientation of the peptide places arginine residues in a position that only allows them to interact with the outermost choline group, thereby preventing favorable guanidinium–phosphate interactions, it is much more likely that the hydrophilic arginine side chains will orient so as to interact with the bulk water, as is the case for Arg^{1} in PG-1. The β-turn arginine residues of PC-13, as in the case of PG-1, exhibit a high affinity for the micelle surface, particularly Arg^{10} and Arg^{11}.

3.3.2.3 PC-9

The RDFs of PC-9 show both of its termini to have a high affinity for the micelle surface. The removal of the disulfide bridge between residues 6 and 15 allows this peptide the flexibility to achieve favorable interactions between arginine residues and the micelle surface at both termini, as well as the cationic region of the β-hairpin turn.

However, this conformation results in an overall bend in the β-hairpin and a curl in the N-terminal strand that places a significant portion of the peptide in the aqueous region, as evidenced by the low lipid peaks (and correspondingly higher water peaks) of residues 4–7. Since Leu^{5} and Ala^{6} are both hydrophobic amino acids,

there is an energetic penalty associated with their presence in the aqueous phase, which would partially offset the favorable interactions achieved for the majority of the arginine residues.

4. Conclusions

The analysis presented has explored two essential features of protegrin-type AMPs: the role of positively charged arginine residues and the effect of the β-hairpin structure in interactions with an amphiphilic environment. The removal of a cationic arginine residue from the C-terminus of PG-1 to yield PC-13 has a significant impact on the membrane-bound conformation of the mutated peptide. As a result of the rigid β-sheet structure of both peptides, interactions at one terminus are able to induce a significant change in the overall orientation of the peptide, and can thus affect interactions in other regions of the peptide. The charged C-terminus in PG-1 binds strongly to the micelle, and orients the overall structure in such a way that interactions between cationic arginine and the anionic phosphate groups of DPC are no longer feasible at the N-terminus. While direct electrostatic repulsions between the two termini may also be responsible for the observed structure of PG-1, the effect just described is believed to be the predominant cause. This is corroborated by a comparison with PC-9, which possesses the same termini as PG-1, yet both its termini reside at the micelle interface and in relatively close proximity to one another, which would not be expected if electrostatic repulsions were high.

The key difference between the sequences of PC-9 and PG-1 is the absence of the Cys^6–Cys^{15} disulfide bond in PC-9, which allows this peptide sufficient flexibility to adopt a conformation that allows it to undergo strong interactions with the micelle at both termini. The resulting structure, although more stable than either PG-1 or PC-13, is significantly distorted from the β-hairpin motif. Unlike in the case of PG-1, the binding of one of the termini to the micelle surface does not result in a change in the overall orientation of the peptide, since the backbone of PC-9 is much more flexible. Furthermore, as evidenced by the relative proximity of the termini of PC-9, the electrostatic repulsions between the charged arginine residues are not sufficient to cause a spreading of the two hairpin strands, as observed in PG-1. It appears that the electrostatic repulsions between the cationic residues can be overcome by reorientation of the arginine sidechains, rather than flexing of the entire backbone in that region; furthermore, since both termini reside in the zwitterionic interface, charge screening effects would further ameliorate the electrostatically unfavorable proximity of the cationic termini. It is therefore believed that the cooperative effect between charged residues and overall reorientation due to the rigidity of the β-sheet structure is primarily responsible for the different behaviour of these peptides.

While simulations of only three peptides with a highly simplified membrane mimic are insufficient to draw meaningful correlations between activity and toxicity, we should like to point out some possible connections. As noted in the introduction, both PG-1 and PC-13 have similar toxicity towards both human red blood cells and epithelial cells, while PC-9 exhibits significantly reduced toxicity. An experimental investigation carried out by Mani *et al.* [49] found that the loss of the β-sheet structure by removal of both disulfide bonds was far more effective in reducing peptide activity than the removal of half of the cationic charges. As such, the β-sheet motif is likely the predominant feature required for peptide activity (and presumably toxicity). The distortion of this motif exhibited by PC-9 in the presence of a DPC micelle in our simulations is consistent with the conclusions of Mani *et al.*, as well as its tested toxicity. In contrast, despite the difference in charge between PG-1 and PC-13, their toxicity measurements are very similar. One possible explanation that emerges from the simulations is that PC-13 does not suffer from the terminus-splitting effect described for PG-1, and as such retains a configuration that is slightly more amenable to membrane insertion. This could potentially offer it increased potency against mammalian membranes over PG-1, which would offset the loss of one unit of charge.

While it is not fully clear how the structural features and interactions observed relate to the biological function of the peptides in question, the present work serves to demonstrate the power of molecular dynamics simulations to elucidate complex biomolecular interactions in atomic detail. The use of such simulations can prove an invaluable tool in further investigations into the mechanisms of action of protegrin and other AMPs, and ultimately in the design of optimal drug candidates.

Acknowledgements

This work was supported by grants from NSF (EEC-0234112) and NIH (GM 070989). Computational support from the Minnesota Supercomputing Institute (MSI) is gratefully acknowledged. This work was also partially supported by National Computational Science Alliance under MCA04N033S and utilized the National Science Foundation HP GS1280 system and the National Science Foundation Terascale Computing System at the Pittsburgh Supercomputing Center. We thank Prof. Alan Waring and Prof. Robert Lehrer for useful discussions.

References

[1] M. Zasloff. Antimicrobial peptides of multicellular organisms. *Nature*, **415**, 389 (2002).
[2] M. Zasloff. Magainins, a class of antimicrobial peptides from Xenopus skin: isolation, characterization of two active forms, and partial cDNA sequence of a precursor. *Proc. Natl. Acad. Sci. USA*, **84**, 5449 (1987).
[3] H. Jenssen, P. Hamill, R.E.W. Hancock. Peptide antimicrobial agents. *Clin. Microbiol. Rev.*, **19**, 491 (2006).

[4] Z. Wang, G. Wang. ADP: the antimicrobial peptide database. *Nucl. Acids Res.*, **32**, D590 (2004).

[5] V. Morell. Antibiotic resistance: road of no return. *Science*, **278**, 575 (1997).

[6] R.M. Epand, H.J. Vogel. Diversity of antimicrobial peptides and their mechanisms of action. *Biochim. Biophys. Acta*, **1462**, 11 (1999).

[7] Y. Ge, D.L. MacDonald, K.J. Holroyd, C. Thornsberry, H. Wexler, M. Zasloff. *In vitro* antibacterial properties of pexiganan, an analog of magainin. *Antimicrob. Agents Chemother.*, **43**, 782 (1999).

[8] K.V. Reddy, R.D. Yedery, C. Aranha. Antimicrobial peptides: premises and promises. *Int. J. Antimicrob. Agents*, **24**, 536 (2004).

[9] H.W. Huang. Molecular mechanism of antimicrobial peptides: the origin of cooperativity. *Biochim. Biophys. Acta*, **1758**, 1292 (2006).

[10] R.E. Hancock, A. Patrzykat. Clinical development of cationic antimicrobial peptides: from natural to novel antibiotics. *Curr. Drug Targets Infect. Disord.*, **2**, 79 (2002).

[11] M. Dathe, H. Nikolenko, J. Meyer, M. Beyermann, M. Bienert. Optimization of the antimicrobial activity of magainin peptides by modification of charge. *FEBS Lett.*, **501**, 146 (2001).

[12] H. Khandelia, A.A. Langham, Y.N. Kaznessis. Driving engineering of novel antimicrobial peptides from simulations of peptide–micelle interactions. *Biochim. Biophys. Acta*, **1758**, 1224 (2006).

[13] V.N. Kokryakov, S.S. Harwig, E.A. Panyutich, A.A. Shevchenko, G.M. Aleshina, O.V. Shamova, H.A. Korneva, R.I. Lehrer. Protegrins: leukocyte antimicrobial peptides that combine features of corticostatic defensins and tachyplesins. *FEBS Lett.*, **327**, 231 (1993).

[14] R.L. Fahrner, T. Dieckmann, S.S. Harwig, R.I. Lehrer, D. Eisenberg, J. Feigon. Solution structure of protegrin-1, a broad-spectrum antimicrobial peptide from porcine leukocytes. *Chem. Biol.*, **3**, 543 (1996).

[15] R. Mani, M. Tang, X. Wu, J.J. Buffy, A.J. Waring, M.A. Sherman, M. Hong. Membrane-bound dimer structure of a beta-hairpin antimicrobial peptide from rotational-echo double-resonance solid-state NMR. *Biochemistry*, **45**, 8341 (2006).

[16] C. Roumestand, V. Louis, A. Aumelas, G. Grassy, B. Calas, A. Chavanieu. Oligomerization of protegrin-1 in the presence of DPC micelles. A proton high-resolution NMR study. *FEBS Lett.*, **421**, 263 (1998).

[17] S. Yamaguchi, T. Hong, A. Waring, R.I. Lehrer, M. Hong. Solid-state NMR investigations of peptide–lipid interaction and orientation of a beta-sheet antimicrobial peptide, protegrin. *Biochemistry*, **41**, 9852 (2002).

[18] D. Gidalevitz, Y. Ishitsuka, A.S. Muresan, O. Konovalov, A.J. Waring, R.I. Lehrer, K.Y. Lee. Interaction of antimicrobial peptide protegrin with biomembranes. *Proc. Natl. Acad. Sci. USA*, **100**, 6302 (2003).

[19] N. Ostberg, Y. Kaznessis. Protegrin structure-activity relationships: using homology models of synthetic sequences to determine structural characteristics important for activity. *Peptides*, **26**, 297 (2005).

[20] R. Mani, S.D. Cady, M. Tang, A.J. Waring, R.I. Lehrer, M. Hong. Membrane-dependent oligomeric structure and pore formation of a beta-hairpin antimicrobial peptide in lipid bilayers from solid-state NMR. *Proc. Natl. Acad. Sci. USA*, **103**, 16242 (2006).

[21] B. Roux. Commentary: surface tension of biomembranes. *Biophys. J.*, **71**, 1346 (1996).

[22] F. Jahnig. What is the surface tension of a lipid bilayer membrane? *Biophys. J.*, **71**, 1348 (1996).

[23] S.E. Feller, R.W. Pastor. On simulating lipid bilayers with an applied surface tension: periodic boundary conditions and undulations. *Biophys. J.*, **71**, 1350 (1996).

[24] J. MacKerell, D. Bashford, M. Bellott, R.L. Dunbrack Jr., J.D. Evanseck, M.J. Field, S. Fischer, J. Gao, H. Guo, S. Ha, D. Joseph-McCarthy, L. Kuchnir, K. Kuczera, F.T.K. Lau, C. Mattos, S. Michnick, T. Ngo, D.T. Nguyen, B. Prodhom, I. Reiher, B. Roux, M. Schlenkrich, J.C. Smith, R. Stote, J. Straub, M. Watanabe, J. Wiorkiewicz-Kuczera, D. Yin, M. Karplus. All-atom empirical potential for molecular modeling and dynamics studies of proteins. *J. Phys. Chem. B*, **102**, 3586 (1998).

[25] S.E. Feller, R.W. Pastor. Constant surface tension simulations of lipid bilayers: the sensitivity of surface areas and compressibilities. *J. Chem. Phys.*, **111**, 1281 (1999).

[26] Y.H. Zhang, S.E. Feller, B.R. Brooks, R.W. Pastor. Computer simulation of liquid/liquid interfaces. I. Theory and application to octane/water. *J. Chem. Phys.*, **103**, 10252 (1995).

[27] F. Castro-Roman, R.W. Benz, S.H. White, D.J. Tobias. Investigation of finite system-size effects in molecular dynamics simulations of lipid bilayers. *J. Phys. Chem. B Condens. Matter. Mater. Surf. Interfaces Biophys.*, **110**, 24157 (2006).

[28] C. Fernandez, K. Wuthrich. NMR solution structure determination of membrane proteins reconstituted in detergent micelles. *FEBS Lett.*, **555**, 144 (2003).

[29] A.R. Rakitin, G.R. Pack. Molecular dynamics simulations of ionic interactions with dodecyl sulfate micelles. *J. Phys. Chem. B*, **108**, 2712 (2004).

[30] T.C. Wong, S. Kamath. Molecular dynamics simulations of adrenocorticotropin (1–24) peptide in a solvated dodecylphosphocholine (DPC) micelle and in a dimyistoylphosphatidylcholine (DMPC) bilayer. *J. Biomol. Struct. Dyn.*, **20**, 39 (2002).

[31] D.P. Tieleman, D. van der Spoel, H.J.C. Berendsen. Molecular dynamics simulations of dodecylphosphocholine micelles at three different aggregate sizes: micellar structure and lipid chain relaxation. *J. Phys. Chem. B*, **104**, 6380 (2000).

[32] W. Braun, C. Bosch, L.R. Brown, N. Go, K. Wuthrich. Combined use of proton–proton Overhauser enhancements and a distance geometry algorithm for determination of polypeptide conformations. Application to micelle-bound glucagon. *Biochim. Biophys. Acta*, **667**, 377 (1981).

[33] A.A. Langham, N. Kaznessis. Effects of mutations on the C-terminus of protegrin-1: a molecular dynamics simulation study. *Mol. Simul.*, **32**, 193 (2006).

[34] B.R. Brooks, R.E. Bruccoleri, B.D. Olfson, D.J. States, S. Swaminathan, K. Karplus. CHARMM: a program for macromolecular energy, minimization, and dynamics calculations. *J. Comput. Chem.*, **4**, 187 (1983).

[35] A.A. Langham, H. Khandelia, Y.N. Kaznessis. How can a beta-sheet peptide be both a potent antimicrobial and harmfully toxic? Molecular dynamics simulations of protegrin-1 in micelles. *Biopolymers*, **84**, 219 (2006).

[36] H. Khandelia, Y.N. Kaznessis. Molecular dynamics investigation of the influence of anionic and zwitterionic interfaces on antimicrobial peptides' structure: implications for peptide toxicity and activity. *Peptides*, **27**, 1192 (2006).

[37] H. Khandelia, Y.N. Kaznessis. Cation-pi interactions stabilize the structure of the antimicrobial peptide indolicidin near membranes: molecular dynamics simulations. *J. Phys. Chem. B Condens. Matter. Mater. Surf. Interfaces Biophys.*, **111**, 242 (2007).

[38] H.M. Berman, J. Westbrook, Z. Feng, G. Gilliland, T.N. Bhat, H. Weissig, I.N. Shindyalov, P.E. Bourne. The Protein Data Bank. *Nucl. Acids Res.*, **28**, 235 (2000).

[39] W.L. Jorgensen, J. Chandrasekhar, J.D. Medura, R.W. Impey, M.L. Klein. Comparison of simple potential functions for simulating liquid water. *J. Chem. Phys.*, **79**, 926 (1983).

[40] A. Langham, Y. Kaznessis. Simulation of the N-terminus of HIV-1 glycoprotein 41,000 fusion peptide in micelles. *J. Pept. Sci.*, **11**, 215 (2005).

[41] H.C. Andersen. Molecular dynamics simulations at constant pressure and/or temperature. *J. Chem. Phys.*, **72**, 2384 (1980).

[42] S. Nose. A molecular dynamics method for simulations in the canonical ensemble. *Mol. Phys.*, **52**, 255 (1984).

[43] S. Nose, M.L. Klein. Constant pressure molecular dynamics for molecular systems. *Mol. Phys.*, **50**, 1055 (1983).

[44] W.H. Hoover. Canonical dynamics: equilibirum phase–space distributions. *Phys. Rev. A*, **31**, 1695 (1985).

[45] J.P. Ryckaert, G. Ciccotti, H.J.C. Berendesen. Numerical integration of the cartesian equations of motion for a system with constraints: molecule dynamics of *n*-alkanes. *J. Comput. Phys.*, **23**, 327 (1977).

[46] U. Essman, L. Perera, M.L. Berkowitz, T. Darden, H. Lee, L.G. Pedersen. A smooth particle mesh Ewald method. *J. Chem. Phys.*, **103**, 8577 (1995).

[47] H. Khandelia, Y.N. Kaznessis. Molecular dynamics simulations of the helical antimicrobial peptide ovispirin-1 in a zwitterionic dodecylphosphocholine micelle: insights into host-cell toxicity. *J. Phys. Chem. B*, **109**, 12990 (2005).

[48] T. Astley, G.G. Birch, M.G.B. Drew, P.M. Rodger, G.R.H. Wilden. Effect of available volumes on radial distribution functions. *J. Comput. Chem.*, **19**, 363 (1998).

[49] R. Mani, A.J. Waring, R.I. Lehrer, M. Hong. Membrane-disruptive abilities of beta-hairpin antimicrobial peptides correlate with conformation and activity: a 31P and 1H NMR study. *Biochim. Biophys. Acta*, **1716**, 11 (2005).